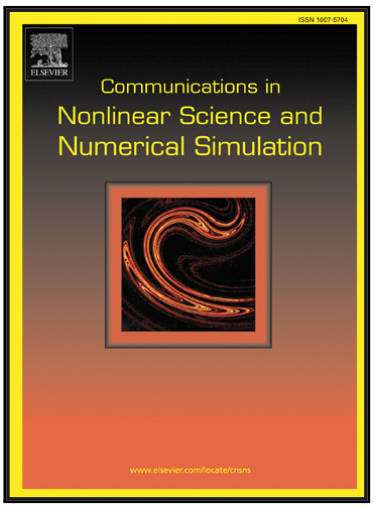

Effect of Gravity-Induced Asymmetry on the Nonlinear Vibration of an Overhung Rotor

Elijah Chipato, A.D Shaw, M.I Friswell

PII: S1007-5704(18)30050-9
DOI: 10.1016/j.cnsns.2018.02.016
Reference: CNSNS 4447

To appear in: *Communications in Nonlinear Science and Numerical Simulation*

Received date: 11 October 2017
Revised date: 24 January 2018
Accepted date: 13 February 2018

Please cite this article as: Elijah Chipato, A.D Shaw, M.I Friswell, Effect of Gravity-Induced Asymmetry on the Nonlinear Vibration of an Overhung Rotor, *Communications in Nonlinear Science and Numerical Simulation* (2018), doi: 10.1016/j.cnsns.2018.02.016

Highlights

- The effect of varying gravity on nonlinear dynamics of an overhung rotor is studied numerically
- Regions of periodic, quasi-periodic and chaotic behaviour shown through methods such as bifurcation analysis and Lyapunov exponent spectra.
- The results presented here show that gravity introduces rich dynamic phenomenon into the rotor. For the zero gravity, case the system only has periodic and quasi-periodic solutions. Upon increasing the gravity parameter, the system now exhibits multi-periodic and chaotic solutions. Rotating frame used to give more insight into the nature of the solutions, particularly for the zero gravity case.
- the isotropic assumption for stiff rotors was found to be reasonably robust in the presence of imperfections since the orbits for the zero gravity case looked quite similar to that of $^{g} = 0.05$ and 0.22.

Effect of Gravity-Induced Asymmetry on the Nonlinear Vibration of an Overhung Rotor

Elijah Chipato, A D Shaw, M I Friswell

College of Engineering, Swansea University Bay Campus, Fabian Way, Crymlyn Burrows, Swansea SA1 8EN, UK

Abstract

In this study a mechanical model of an overhung rotor is explored to determine the effect of gravity on the nonlinear dynamics of an aero-engine. The model is an overhung disc with rotor-stator contact. The model has two degrees of freedom with lumped parameters; friction is neglected in the contact and the equations of motion are non-dimensionalised. A parametric study of the non-dimensional gravity parameter is conducted. The bifurcation plots show that gravity plays a crucial role in the nonlinear dynamics of such systems. With zero gravity, as explored in earlier studies, the model has synchronous whirling solutions, and asynchronous partially contacting solutions that are periodic only when viewed in a rotating coordinate system. If the gravity parameter is non-zero, then the dynamics observed are much richer and show additional multi-periodic and chaotic solutions in the stationary frame and continuous contact (full annular rub).

Keywords: Overhung rotor, Rotor stator contact, Bifurcation, Chaos, Internal resonance

1. Introduction

Rotor stator contact affects many rotating machines from drill strings to aero-engines. In most cases the rub is initiated by static unbalance. There are three major classes of rotating machinery vibrations namely axial, torsional and lateral vibration. For aero engines lateral vibrations are the most destructive type of vibration and can include forward, backward and chaotic whirls. Forward whirl (FW) is synchronous or asynchronous(with contact) and the rotor orbits in the same direction as the rotor spin, whereas backward whirl (BW) is more destructive and characterized by an orbiting rotor opposite to the direction of rotor spin and is initiated by the presence of a large frictional force between rotor and stator. In chaotic whirl there is no preferential orbit of the rotor and it bounces

in any direction. Whirling shafts or rotors can subsequently interact with the stator/enclosure and this rubbing action can also change the nature of the whirl.

Ehrich [1] gave a comprehensive study of a number of rubbing phenomena observed in turbo-machinery, including period two solutions, chaos and subhamornic resonances. Some of these phenomena were also observed in the present study, namely period two and chaos. Vijayan et al. [2] studied the influence of rotor rub on backward whirl of a two disk rotor and found that vibration modes excited in the system can be changed by altering the phase differences between eccentric masses of the two disks and suggested that this controlled the initiation of backward whirl since altering the eccentric masses might initiate continuous rubbing which increases the friction in the system. Zilli et al. [3] examined the dynamics of an overhung rotor to try and understand bouncing motion that had been observed in earlier experiments. The bouncing response was observed to occur away from the primary resonance and the response was found to be composed of three frequency components which are not spaced at harmonic or subhamornic intervals. It was then found out that this bounce response at a constant rotor spin speed was obtained when there was synchronisation between the three distinct frequency components, this then led to the approximate prediction of the rotor spin speeds at which such bouncing motions can be predicted. Shaw et al. [4] suggested that bouncing periodic motion can be initiated by an internal resonance condition in the system and stressed that this internal resonance condition is only considered as a necessary rather than sufficient condition for the onset of this motion; this motion was termed asynchronous partial contact orbits.

In other work, Zhou et al. [5] studied a nonlinear model of a rotor seal system including the coupled effects of gravity, Muszynska's nonlinear seal fluid dynamic force and mass eccentricity. The system was analysed using bifurcation diagrams, time history plots, orbit plots, Poincaré maps and spectra and as the rotational speed is increased rich forms of dynamic behaviour were found including periodic, multi-periodic, quasi periodic and chaotic dynamic motion. The effects of seal drop pressure, seal length, seal clearance, distance between the two disks and mass of the discs on the dynamics of the system was investigated and it was found that high seal drop pressure, an optimised seal clearance, long seal length and a symmetrical disc structure can enhance the stability of a double disc rotor-seal system.

Hui et al. [6] performed a comprehensive study of oil film instability in an overhung rotor system with flexible coupling misalignment. A finite element model of the overhung rotor system with gyroscopic effects was used and sliding bearings were simulated using a nonlinear oil film force

model using the assumption of short-length bearings. The finite element model was validated using experimental data. Their study shows that under perfectly aligned conditions, the onset of first and second vibration mode instability in a run down are less than during run up due to the hysteresis effect, this can also be viewed as the presence of multiple solutions, with different initial conditions finding different solutions. When misaligned there was a delay in the onset of the first vibration mode instability and this resulted in a decrease in the vibration amplitude.

Yang et al. [7] used time-frequency techniques for rub-impact detection in rotating machinery. The authors introduced a new method based on the fast oscillation characteristics of instantaneous frequency to detect rub-impact faults of rotor bearing systems. A fast time varying transient stiffness (stiffening effect) of rub impact was formulated and a time frequency technique called the nonlinear squeezing time frequency transform was introduced to extract the instantaneous frequency. They show that the instantaneous frequency of the vibration response remained constant at the rotor spin speed if there is no rub-impact fault. However, the instantaneous frequency oscillated periodically around the basic harmonic frequency (rotor spin frequency) whenever a rub impact fault occurred. Their proposed new analysis method was also validated using experiments.

Wang et al. [8] investigated the sudden unbalance and rub-impact caused by a blade off scenario in an overhung rotor and used both theoretical and experimental approaches to study the system. Their results reveal that the sudden unbalance caused by blade loss will introduce an impact effect in the rotor and the frequency spectrum shows that the first critical speed frequency (including the backward whirling frequency) appears. Also, the authors noted that rubbing action between the rotor and constraint ring induces a load path to absorb the unbalance loads and generates additional stiffness which causes the resonance speed to rise and the resonance region to expand.

Other authors have also reported significant research on the rub impact problem. Comprehensive experimental work was done by [9–13] to try and understand the rotor-stator contact problem. Jiang and Chen [14] summarised the literature on rotor stator rubbing based on work that has been done in the past half century from the point of view of dynamics and control. Ehrich [15] found that high speed rotors with bearing clearance exhibit very high orders of subharmonic vibration particularly for systems with low damping and extreme nonlinearity. The analysis of nonlinear motions with rub have also been classified using bifurcation plots, time series analysis, rotor orbits, Poincaré sections and the response spectra [16–20].

Rotors can be classified into two categories namely vertical shaft systems and horizontal shaft

systems. Normally for vertical shaft systems, the effect of gravity can be ignored but for Horizontal shaft systems the effect of gravity has to be checked, although most researchers do not justify why gravity is neglected in their modelling [21, 22]. The main reason for including gravity in horizontal shaft systems is that they are susceptible to a gravity sag. Also even when gravity is ignored we see very interesting phenomena happening. In this paper we intend to unravel how these interesting phenomena evolve as gravity effects become stronger. An overhung rotor model is presented and the equations of motion are derived using the Lagrange method. The 4th order Runge-Kutta method is employed to calculate the nonlinear response of the system. Bifurcation diagrams for different rotor speeds while varying the gravity parameter are used to identify the values of the gravity parameter with potentially interesting solutions. Then bifurcation diagrams with rotor spin speed for different values of the gravity parameter are plotted with their corresponding Lyapunov exponents to characterize the nature of the solutions particularly for chaos. Vibration responses, orbit trajectories, Poincaré maps and amplitude spectra in stationary and rotating frames are presented and a discussion of the effect of gravity is given.

2. Theoretical model

This study uses a lumped parameter model of an overhung rotor which is described using ordinary differential equations. This finite dimensional representation of the system provides a good description of the dynamics experienced by a stiff rotor with flexible supports. In this work a two degree of freedom system model is formulated which is inspired by the work of Zilli et al. [3].

The idealized model is shown in Figure 1. For a more detailed description of the system the reader is referred to [3]. Using the Lagrange formulation the equations of motion are derived as [3]

$$\begin{cases} J_s\ddot{\phi_y} - J_p\dot{\theta}\dot{\phi_x} + D\dot{\phi_y} + k_\phi\phi_y = ame(\dot{\theta}^2\cos\theta + \ddot{\theta}\sin\theta) + M_{\phi_y} \\ J_s\ddot{\phi_x} + J_p\dot{\theta}\dot{\phi_y} + D\dot{\phi_x} + k_\phi\phi_x = ame(\ddot{\theta}\sin\theta - \dot{\theta}^2\cos\theta) + M_{\phi_x} + amg \end{cases} \tag{1}$$

where ϕ_x and ϕ_y are rotations about the x and y axes respectively, m is the mass of disk, g is the acceleration due to gravity, θ is the rotation angle, J_s is the equivalent moment of inertia of the overhung rotor system and is given by $J_s = (J_t + a^2m)$, J_t is the transverse moment of inertia, J_p is the polar moment of inertia, e is mass unbalance eccentricity, M_{ϕ_x} and M_{ϕ_y} are the generalized

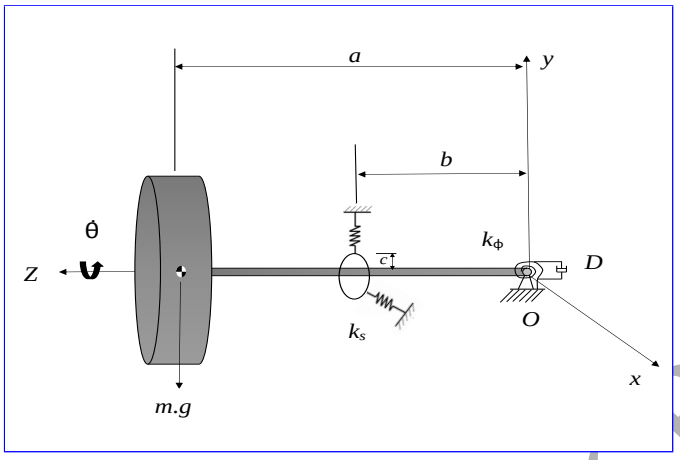

Figure 1: **Schematic of overhung rotor**

moments associated with the normal snubbing force F_n where friction is ignored and are given by

$$M_{\phi_y} = H(||r_c|| - c^*)k_s b^2 \phi_y \left(\frac{c}{b\sqrt{\phi_x^2 + \phi_y^2}} - 1 \right) \tag{2}$$

$$M_{\phi_x} = H(||r_c|| - c^*)k_s b^2 \phi_x \left(\frac{c}{b\sqrt{\phi_x^2 + \phi_y^2}} - 1 \right) \tag{3}$$

$H(||r_c|| - c^*)$ is a heaviside step function which activates Equations (2) and (3) when there is contact in the system and introduces non-linearities in the equations of motion, r_c is the radial displacement of disk's center, c is the radial clearance and $c^* = \frac{ca}{b}$ is the displacement of the disk centre that leads to contact. Equations (1) can be nondimensionalised, which reduces the number of parameters by lumping them together into dimensionless groups which also simplifies the analysis [23]. The equations of motion of this system are given in the dimensionless form [3] where a caret ($\hat{}$) and apostrophe ($'$) represents a nondimensional quantity and a derivative with respect to nondimensional time respectively. Nondimensional time is given by $\tau = \omega_n t$, where $\omega_n^2 = k_\phi / J_s$,

and the rotations are scaled as $\hat{\phi_x} = \phi_x \frac{a}{c^*}$ and $\hat{\phi_y} = \phi_y \frac{a}{c^*}$. Thus

$$\begin{cases} \hat{\phi}_y'' - \hat{J}_p \theta' \hat{\phi}_x' + 2\zeta \hat{\phi}_y' + \hat{\phi}_y = \hat{m}\hat{e}(\theta'^2 \cos\theta + \theta'' \sin\theta) + \hat{M}_{\phi_y} \\ \hat{\phi}_x'' + \hat{J}_p \theta' \hat{\phi}_y' + 2\zeta \hat{\phi}_x' + \hat{\phi}_x = \hat{m}\hat{e}(\theta'' \sin\theta - \theta'^2 \cos\theta) + \hat{M}_{\phi_x} + \hat{m}\hat{g} \\ \hat{M}_{\phi_y} = H(||\hat{r_c}|| - 1)\beta\hat{\phi}_y \left(\frac{1}{\sqrt{\hat{\phi}_x^2 + \hat{\phi}_y^2}} - 1 \right) \\ \hat{M}_{\phi_x} = H(||\hat{r_c}|| - 1)\beta\hat{\phi}_x \left(\frac{1}{\sqrt{\hat{\phi}_x^2 + \hat{\phi}_y^2}} - 1 \right) \end{cases} \tag{4}$$

where $\hat{g} = \frac{g}{c^* \omega_n^2}$, $\hat{m} = \frac{ma^2}{J_s}$, $\hat{e} = e/c^*$, β is the ratio between snubbing stiffness and the linear stiffness of the rotor, $\frac{k_s}{k_r}$, and $k_r = \frac{k_\phi}{b^2}$. The gravity parameter $\hat{g}$ depends on the ratio of the gravity force to the rotor stiffness, and hence depends on the static deflection of the rotor due to gravity. For example, if J_t is negligible, so that $\hat{m} = 1$, then if $\hat{g} = 1$ the stationary rotor just touches the stator with the static deflection due to gravity. The gravity parameter also introduces asymmetry into the rotor. Although gravity can be neglected for vertical shaft systems, often gravity is neglected for horizontal shaft systems without any justification. Varney and Green [17] highlighted that gravity has a significant effect on the response of nonlinear rotor systems, particularly at low rotational speeds, which corresponds to the low stiffness case identified here. For systems with very stiff rotors, such as aero engines, gravity can be neglected ($\hat{g} \approx 0$). At the opposite extreme, drill strings have very flexible rotors, and gravity becomes significant when the bore is only slightly non-vertical.

3. Numerical analysis and results

The numerical analysis in this study used the fourth order Runge-Kutta numerical method with an adaptive step control to lower the local truncation error. Representative test parameters are shown in Table 1 following the studies made by Zilli et al. [3]. The numerical calculation used the ODE45 solver in MATLAB for a given initial condition, where the events function was used to identify the exact point where contact is made which will trigger the step control mechanism to reduce the step size for accuracy during contact. To perform numerical calculations it is convenient to transform Equation (4) into state space form.

3.1. Bifurcation Analysis

Bifurcation diagrams show the qualitative changes that occur as a system parameter is varied. In rotordynamics, rotor spin speed has a great impact on the dynamics of rotating machinery mainly

Table 1: **Nondimensionalised system parameters**

Symbol	Parameter	Value
$\hat{m}$	Normalised mass	0.9285
$\hat{J}_p$	Normalised polar moment of inertia	0.143
β	Stiffness nonlinearity	1.32
$\hat{e}$	Normalised rotor eccentricity	0.494
ζ	Damping ratio	0.01

because it determines the magnitude of the unbalance force, for an unbalanced rotor system it is the excitation frequency and that in the presence of gyroscopic effects it causes a frequency split between FW and BW vibration frequencies. In this study both the dimensionless rotor spin speed, $\hat{\Omega}$, and the gravity parameter, $\hat{g}$, are used as control parameters. Figure 2 shows bifurcation diagrams where $\hat{g}$ is varied for two different rotor spin speeds which lie inside and outside the contacting region for the zero gravity case studied by [3]. This enables the values of $\hat{g}$ with interesting solutions to be studied. Figure 2a is for $\hat{\Omega}$ outside the bistability region and for $\hat{g}$ less than 1.2 there is only one value of radial displacement for a given value of $\hat{g}$ showing that the system is periodic. The system then bifurcates into period 2 solutions and then back to period one solutions. For the bifurcation diagram for $\hat{\Omega}$ inside the contacting region shown in Figure 2b, we see that for the range $\hat{g}$ is less than 1.28 there is an interchange between periodic motion and non periodic motion. Later, the Lyapunov spectrum for $\hat{g}$ in these non-periodic regions will prove that this in fact evidence of the existence chaotic solutions. It is also important to note that Figure 2 also shows that for high values of $\hat{g}$ the rotor remains in contact with the stator (full annular rub) and that static displacements due to gravity begin to dominate the response. From Figure 2 values of $\hat{g}$ of 0, 1.27, 2.14 and 3.44 were chosen for further study. It is important to note that the zero gravity case, $\hat{g} = 0$ was studied in [3]. Figure 3 shows the bifurcation analysis for the effect of rotational speed, $\hat{\Omega}$, on the dynamics of the overhung rotor system for different values of $\hat{g}$. Each bifurcation diagram for each gravity case has been plotted for two sets of initial conditions, firstly using random initial conditions and then doing a sweep up that takes the final state of a simulation at a given value of $\hat{\Omega}$ as the initial condition of the next simulation. This type of representation demonstrates one property of nonlinear systems which is the existence of multiple solutions.

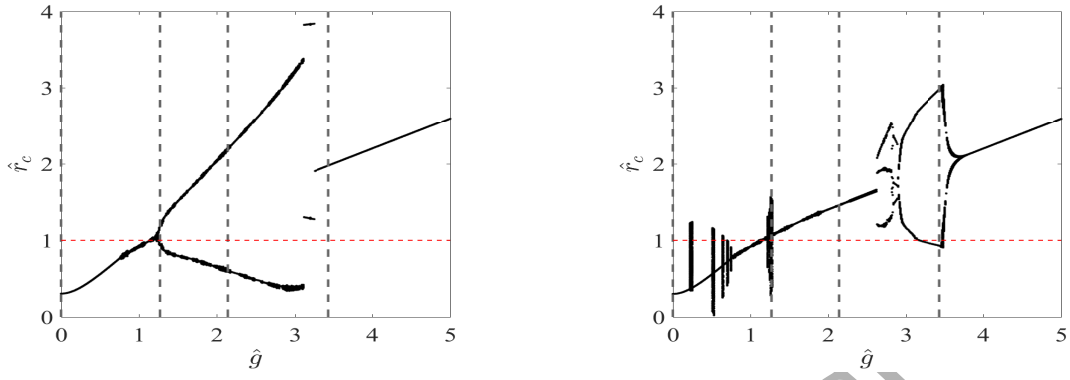

(a) $\hat{\Omega} = 3.20$ (b) $\hat{\Omega} = 3.38$

Figure 2: **The bifurcation plots with $\hat{g}$ as control parameter for two rotor spin speeds. Vertical dashed lines show the value of $\hat{g}$ chosen for further studies. The horizontal dashed lines indicate the clearance, and hence when the rotor is in contact with the stator.**

Bifurcation diagrams might appear to show chaos in many cases but often these cases are actually quasi-periodic/ asynchronous rather than truly chaotic. Therefore, to characterize the dynamics of the system more conclusively, particularly for chaos, the largest Lyapunov exponent spectra for the four cases are computed [24, 25] and shown in Figure 4. The largest Lyapunov exponents give a direct measure of sensitive dependence on initial conditions (SDIC) [23, 24, 26]. A positive largest Lyapunov exponent shows that there is chaotic motion on a strange attractor. If the largest Lyapunov exponent is zero then we have periodic/ quasi-periodic motion and if the largest Lyapunov exponent is negative then the stable critical point is an attractor [27]. From Figure 4a, which is the zero gravity case, it is observed that the Lyapunov exponents of the system are mostly negative and we see that in the regions where quasi periodic solutions are present the lyapunov exponent approaches zero .

However, increasing the gravity parameter, for example to 0.05, the bifurcation diagram appears a little different from the zero gravity case and more increase to 0.22, 1.27 and 2.14 results in richer dynamics of the system being observed and now includes chaos and multi-periodic solutions(period 2, period 3, etc). As the gravity parameter was further increased to 3.44, it was noted that no chaos was detected although the dynamics are still richer than the zero gravity case with regions of period two solutions. In this case the static deflection due to gravity dominates the response

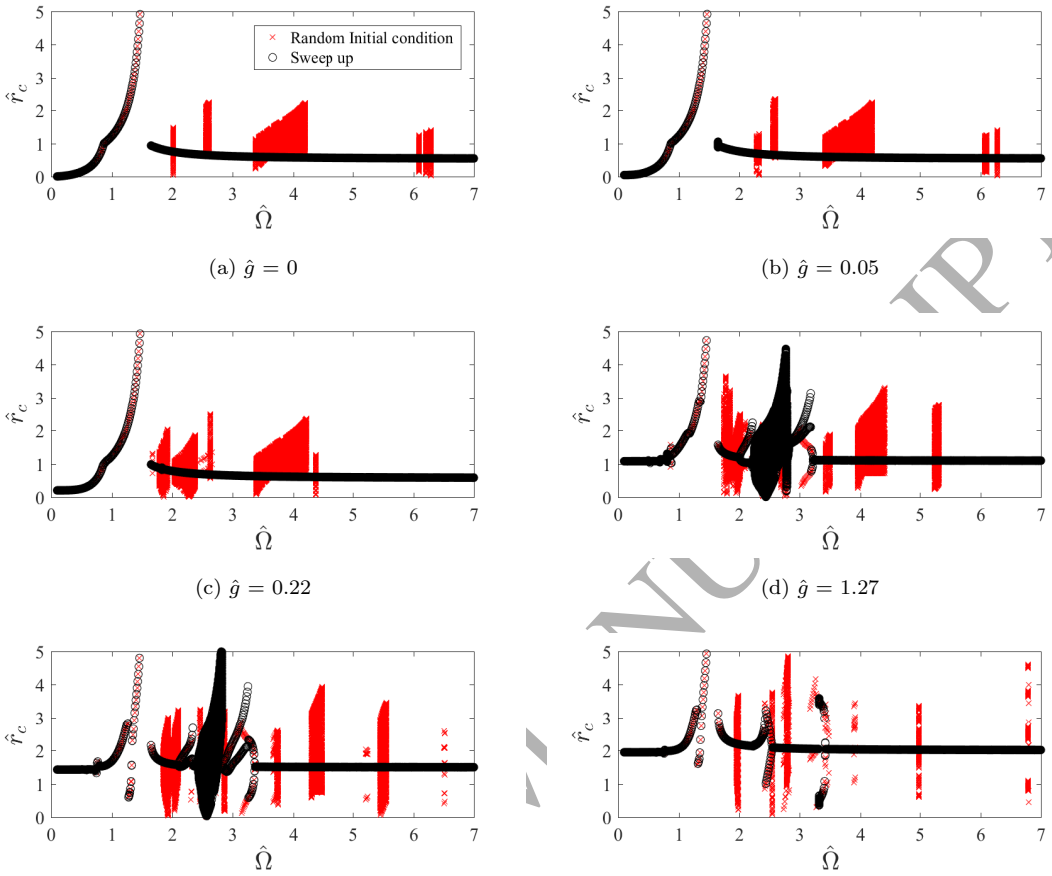

(a) $\hat{g} = 0$ (b) $\hat{g} = 0.05$

(c) $\hat{g} = 0.22$ (d) $\hat{g} = 1.27$

(e) $\hat{g} = 2.14$ (f) $\hat{g} = 3.44$

Figure 3: **The bifurcation plots with rotor spin speed for different values of $\hat{g}$.**

and full annular rub is often experienced. However the rotor still has solutions where it bounces in and out of contact. Figure 5 shows the vibration responses, orbit trajectories, Poincaré maps and amplitude spectra in both the stationary and rotating frames for $\hat{\Omega} = 3.47$ for $\hat{g} = 0$. Figure 5b shows that the motion is not periodic when viewed in the stationary frame as the orbit shows that the rotor is in continuous precession. However, viewing the motion in the rotating frame shows that the motion is rather simple and periodic [4]. To better understand the response an FFT of the rotation, in the stationary,ϕ_x and rotating frames, $\tilde{\phi_x}$ is taken. In the stationary frame three peaks are observed at 3.47, 1.319 and 0.856. The dominant frequency corresponds to the rotor

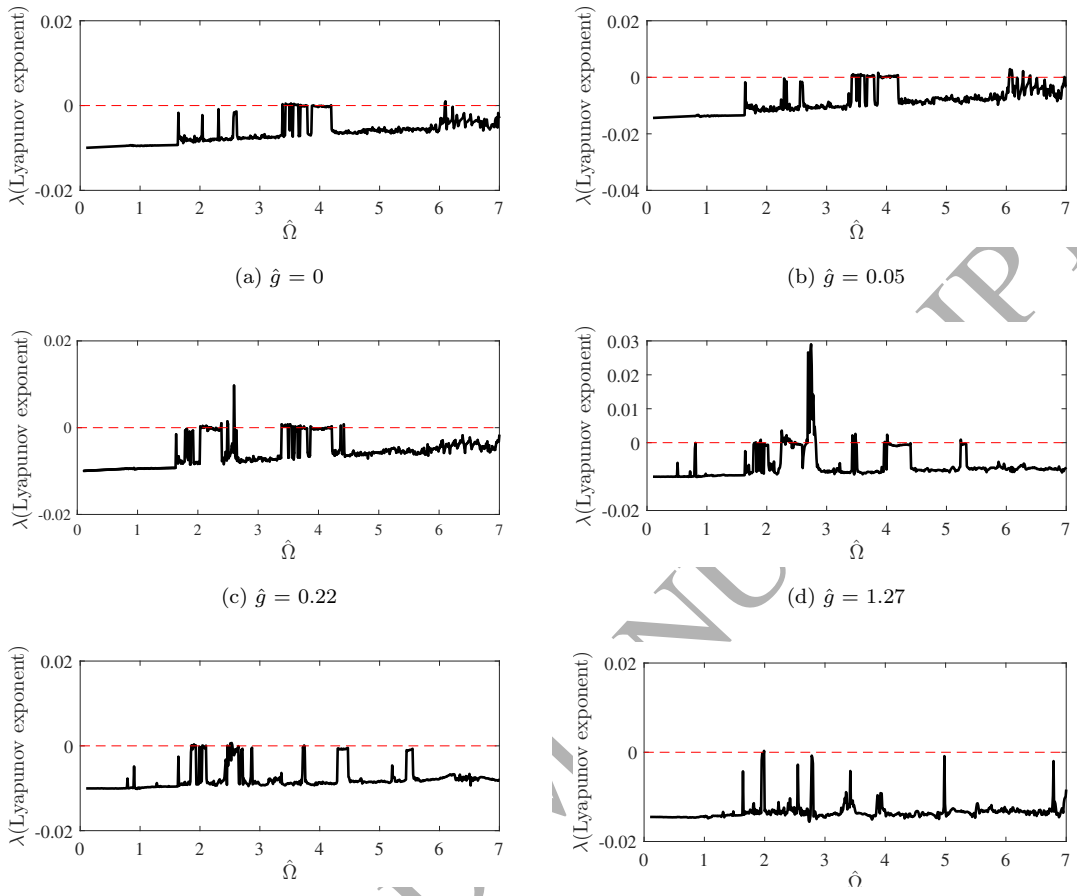

(a) $\hat{g} = 0$ (b) $\hat{g} = 0.05$

(c) $\hat{g} = 0.22$ (d) $\hat{g} = 1.27$

(e) $\hat{g} = 2.14$ (f) $\hat{g} = 3.44$

Figure 4: **The largest Lyapunov spectra for different values of $\hat{g}$.**

spin speed/ excitation frequency and the other two frequencies correspond to the first forward and backward whirling frequencies as shown in the Campbell diagram in Figure 6. The value of the forward and backward whirling frequencies at a reference speed of 3.47 is found to be 1.2784 and 0.7822 and are slightly lower than the values obtained from the FFT by 3% and 9% respectively. Since the frequencies obtained from the Campbell diagram are lower than that of the FFT this can be regarded as a stiffening effect induced by the stator.

However , something more interesting happens in the rotating frame. The peaks obtained from Figure 5h are 2.151 and 4.326 and these two frequencies are in a 2:1 ratio approximately. The

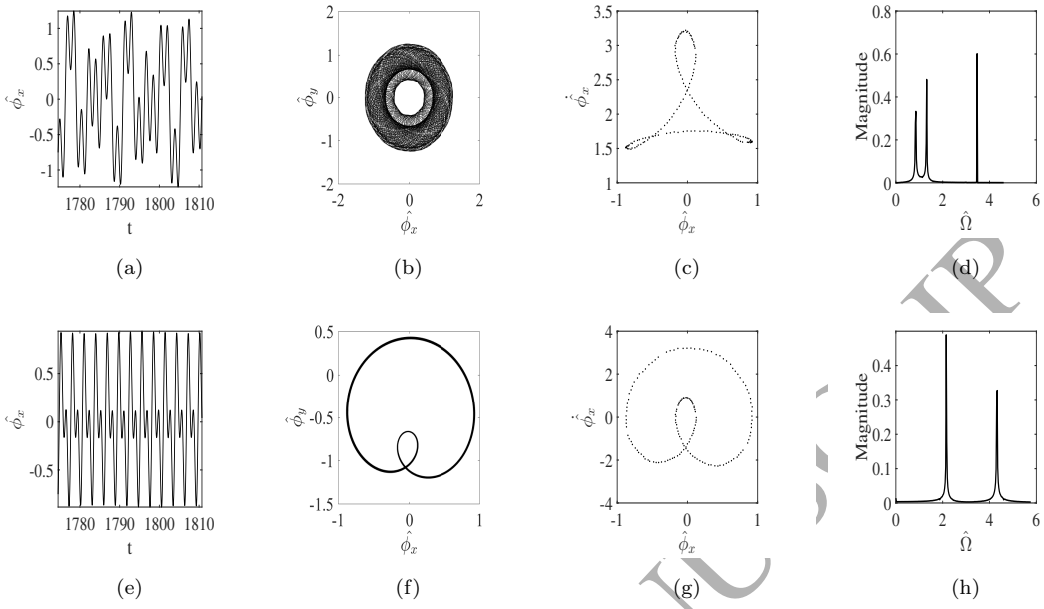

Figure 5: **Vibration responses (5a and 5e), phase trajectories (5b and 5f), Poincaré maps (5c and 5g) and amplitude spectra (5c and 5g) for $\hat{\Omega} = 3.47$ for the zero gravity case, $\hat{g} = 0$. Figures (5a - 5d) are for stationary frame and figures (5e - 5h) are for the rotating frame of reference.**

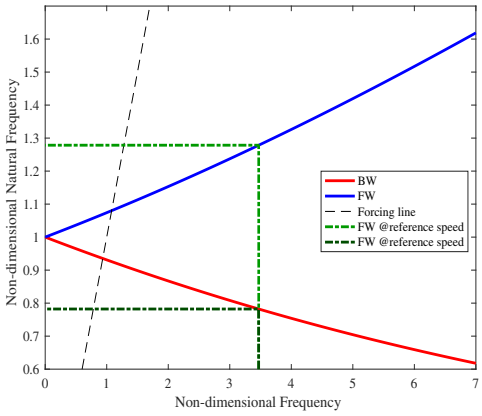

Figure 6: **Campbell diagram showing forward and backward whirl speed at reference rotor spin speed $\hat{\Omega} = 3.47$**

FFT of the response in the rotating frame only shows two peaks, unlike that for the stationary frame which has three peaks. In the rotating frame the unbalance force is not harmonic but static and therefore the third peak in the FFT for the stationary frame, which represents the rotor spin frequency, does not appear in the FFT for the rotating frame. Note that the Poincaré section in Figure 5g does not show two isolated points because the sampling rate is determined by the rotor spin speed, whereas the periodicity of the response is determined by the natural frequencies in the rotating frame. By definition, in the stationary frame BW is negative and FW is positive. In the rotating frame the same applies but when the natural frequencies are less than the rotor spin speed then both BW and FW are negative. The whirl velocities in the stationary frame can be related to that of the rotating frame by [4],

$$\hat{w_s} = \hat{w_r} + \hat{\Omega} \tag{5}$$

where $\hat{w_r}$ is the whirling velocity in rotating frame and $\hat{w_s}$ is the whirling velocity in stationary

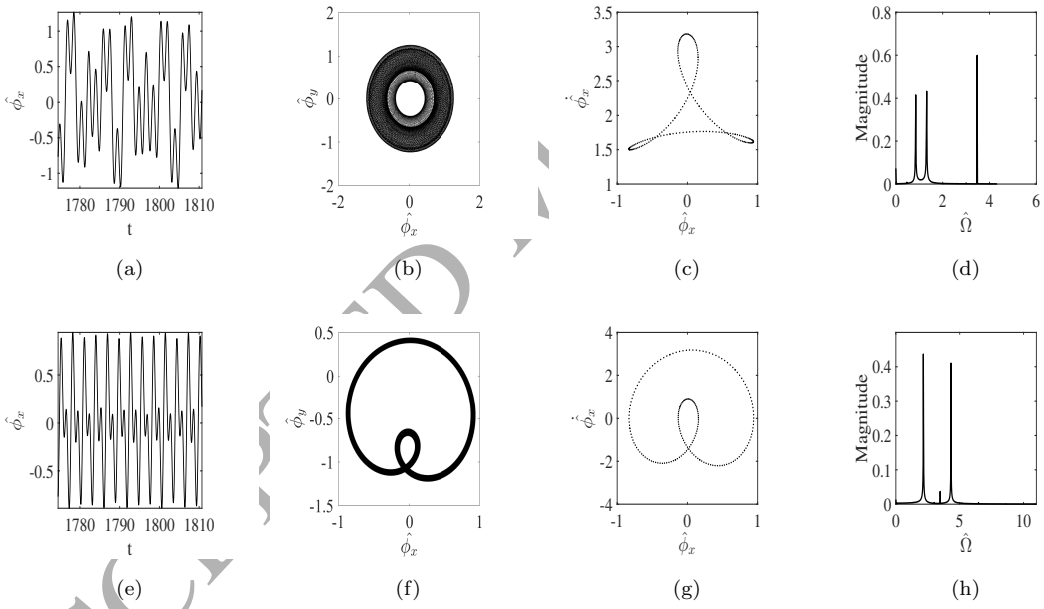

Figure 7: **Vibration responses (7a and 7e), phase trajectories (7b and 7f), Poincaré maps (7c and 7g) and amplitude spectra (7h and 7d) for $\hat{\Omega} = 3.47$ for $\hat{g} = 0.05$. Figures (7a - 7d) are for stationary frame and Figures (7e - 7h) are for the rotating frame of reference.**

frame. This therefore shows that to convert the frequencies obtained from the FFT for the rotating

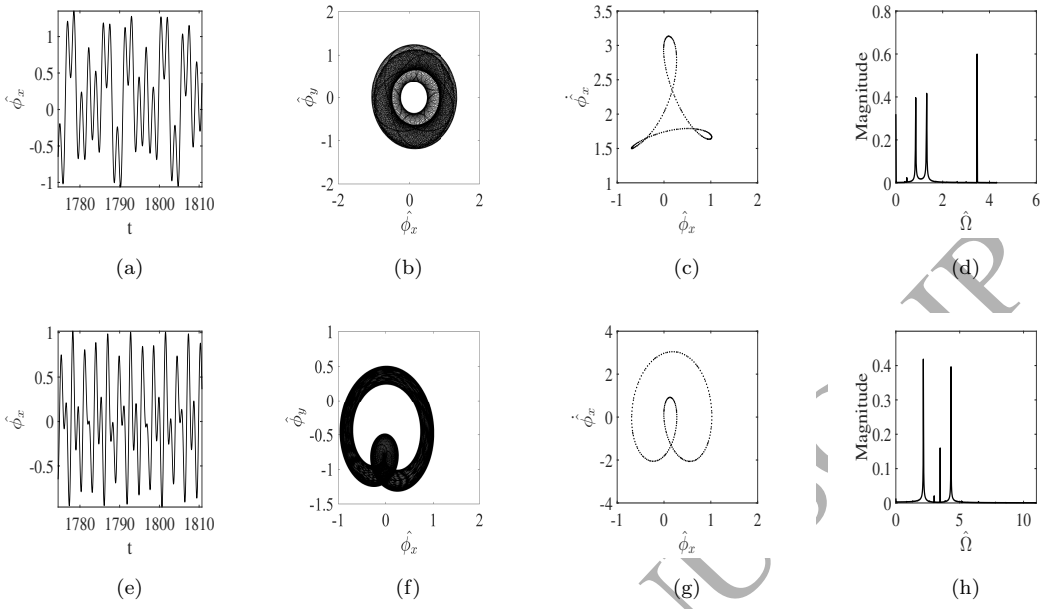

Figure 8: **Vibration responses (8a and 8e), phase trajectories (8b and 8f), Poincaré maps (8c and 8g) and amplitude spectra (8h and 8d) for $\hat{\Omega} = 3.47$ for $\hat{g} = 0.22$. Figures (8a - 8d) are for stationary frame and Figures (8e - 8h) are for the rotating frame of reference.**

frame one should add the rotor spin speed. This then gives 0.856 = (4.326-3.47) and -1.319 = (2.151-3.47) which corresponds to the values obtained from the FFT of the stationary frame. The fact that both the forward and backward whirling frequencies are present in both frames shows that there is an interaction/ energy exchange taking place between the FW mode and the BW mode that is to say an internal resonance.

Figures 3b and 3c shows bifurcations for $\hat{g} = 0.05$ and 0.22. The two gravity cases were used to check the robustness of the zero gravity case. Figures 7b and 8b shows the orbit for $\hat{g} = 0.05$ and 0.22 at 3.47 (similar to Figure 5), here we see that the isotropic assumption is reasonably robust in the presence of imperfections which are introduced by the inclusion of gravity since the orbits visualised in stationary frame look quite similar to that of the zero gravity case (Figure 5b). The orbits visualised in the rotating frame for the two gravity cases shown in Figures 7f and 8f are similar to Figure 5f, however they deviate from this orbit due to the gravity force, which is not constant in the rotating frame.

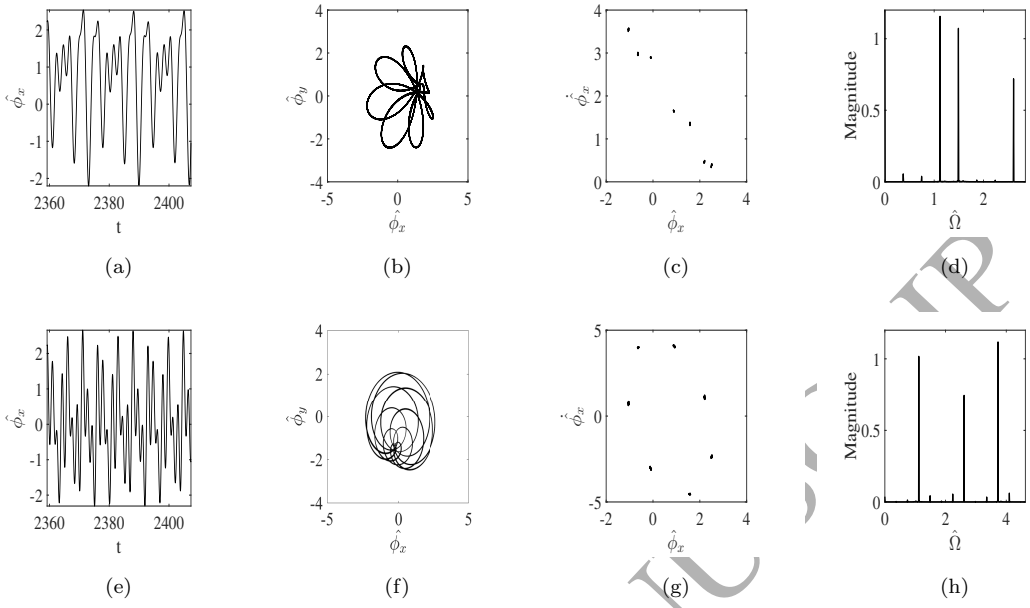

Figure 9: **Vibration responses (9a and 9e), phase trajectories (9b and 9f), Poincaré maps (9c and 9g) and amplitude spectra (9d and 9h) for $\hat{\Omega} = 2.61$ for $\hat{g} = 1.27$. Figures (9a - 9d) are for stationary frame and figures (9e - 9h) are for the rotating frame of reference.**

Figure 4d shows the largest Lyapunov spectrum for $\hat{g} = 1.27$ and shows that gravity introduces some chaos into the system since at rotor spin speeds 2.09, 2.39 and 2.68 to 2.82 the largest Lyapunov exponents are positive. Figure 9 shows period 7 motion and Figure 10 chaotic motion for $\hat{g} = 1.27$ for both stationary and rotating frames. It was noted that the character of the dynamics is the same in both frames, that is, the simplification in the rotating frame (see Figure 5) for $\hat{g} = 0$ does not happen for $\hat{g} = 1.27$. Figure 9a - 9d shows the results for $\hat{\Omega} = 2.61$ for stationary frame. The Poincaré map shown in Figure 9c shows that the motion is period 7, the FFT in Figure 9d shows 3 peaks at 1.114,1.496 and 2.61 which are BW, FW and the excitation frequency (rotor spin speed). The 3 peaks are related in such a way that they give a period 7 response by -3*(1/BW) + 4*(1/FW) = 7*(1/2.61). There is significant difference between the Campbell diagram values and FFT frequency values as compared to the zero gravity case. The reason for this huge difference could be that increasing the gravity parameter will mean that there is more significant contact and therefore more stiffening which results in the FFT values being larger. Also note that the

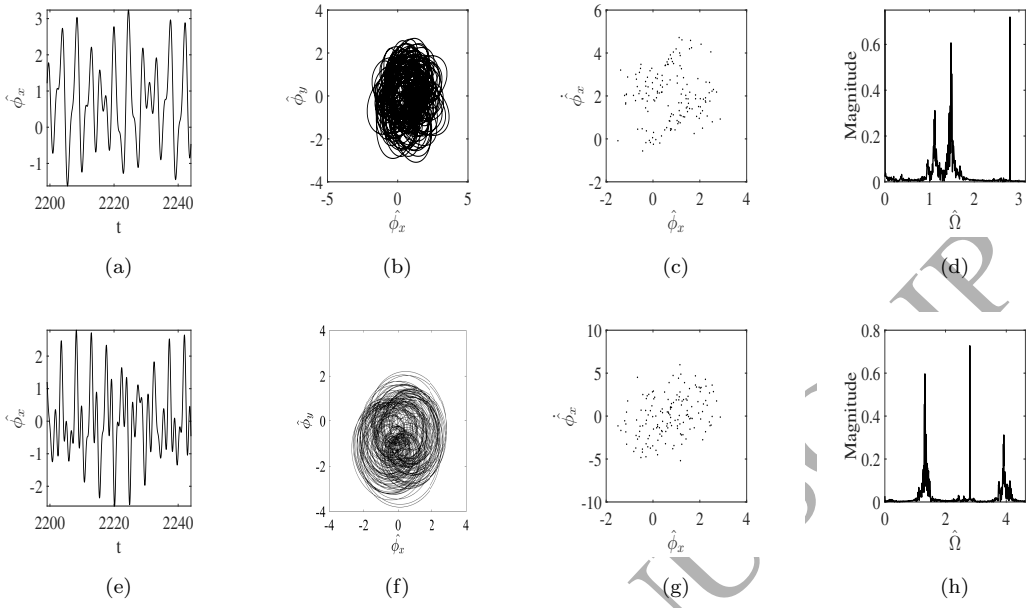

Figure 10: **Vibration responses (10a and 10e), phase trajectories (10b and 10f), Poincaré maps (10c and 10g) and amplitude spectra (10h and 10d) for $\hat{\Omega} = 2.80$ for $\hat{g} = 1.27$. Figures (10a - 10d) are for stationary frame and Figures (10e - 10h) are for the rotating frame of reference.**

FFT for the rotating frame now has 3 peaks unlike for the zero gravity case where it only had two. The reason for this observation is that in the rotating frame the unbalance force is static but gravity is harmonic and therefore the rotor spin frequency peak appears. Figures (10e - 10h) shows the response, orbit, Poincaré map and FFTs obtained for a rotor spin frequency of 2.80 for both stationary and rotating frames. The plots show evidence of chaos as the orbits show strange attractors, the Poincaré maps have points which are distributed in no particular order and the FFTs show a broadband response showing the presence of finite frequency components in the time series signal.

Figure 11 and 12 shows period 2 and period 3 solution for $\hat{g} = 2.14$ at rotational speeds of 2.11 and 5.23 respectively and both motions are visualised in the stationary and rotating frames. Figures 11a and 11b show the time series and the orbit in stationary frame and from this the motion is periodic. The Poincaré map in Figure 11c shows two isolated points and the frequency ratio between the two peaks in the Fourier transform in Figure 11d is 2:1 showing that this solution

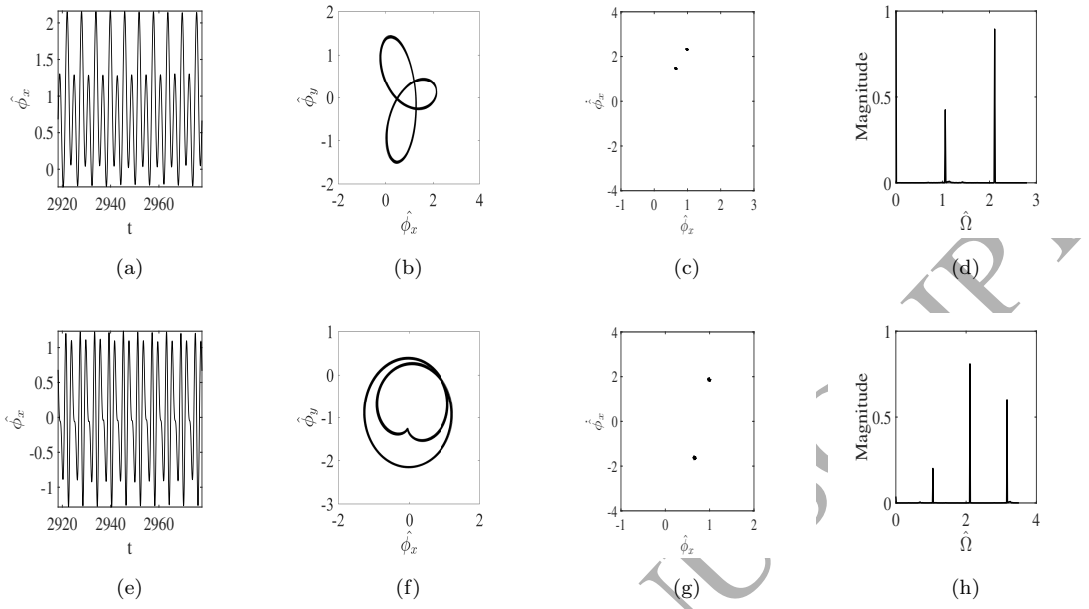

Figure 11: **Vibration responses (11a and 11e), phase trajectories (11b and 11f), Poincaré maps (11c and 11g) and amplitude spectra (11d and 11h) for $\hat{\Omega} = 2.11$ for $\hat{g} = 2.14$. Figures (11a - 11d) are for stationary frame and figures (11e - 11h) are for the rotating frame of reference.**

is indeed period 2 motion. When visualised in the rotating frame, the somewhat complicated orbit in Figure 11b is simplified in 11f and the FFT in Figure 11h shows synchronous peaks at $0.5\hat{\Omega}$, $\hat{\Omega}$ and $3\hat{\Omega}$. Figure 12 shows a period 3 solution, where the Poincaré maps in Figure 12c and 12g now show three isolated points proving that it is period 3. The two major peaks in the FFT visualised in the stationary frame are in ratio of 3:1 and in the rotating frame there are peaks at 3.482, 5.23 and 6.978 with the second and third peak being 1.5 and two times the first peak respectively.

Figure 13 shows the complicated nonlinear motions of the rotor for $\hat{g} = 3.44$ at a rotor spin speed of 2.55. The motion here is also visualised in both frames and as seen in Figures 13b and 13f the orbits in both frames look quite complicated; visualising the motion in the rotating frame did not simplify the orbit. To understand the motion we look at the Lyapunov spectrum, Poincaré maps and amplitude spectra. The Poincaré maps shown in Figures 13c and 13g both show a closed loop, the Lyapunov exponent shown in Figure 4f is approximately zero and the FFTs shown in Figures 13d and 13h show discrete peaks. Thus the complicated nonlinear motion shown here is quasi-periodic.

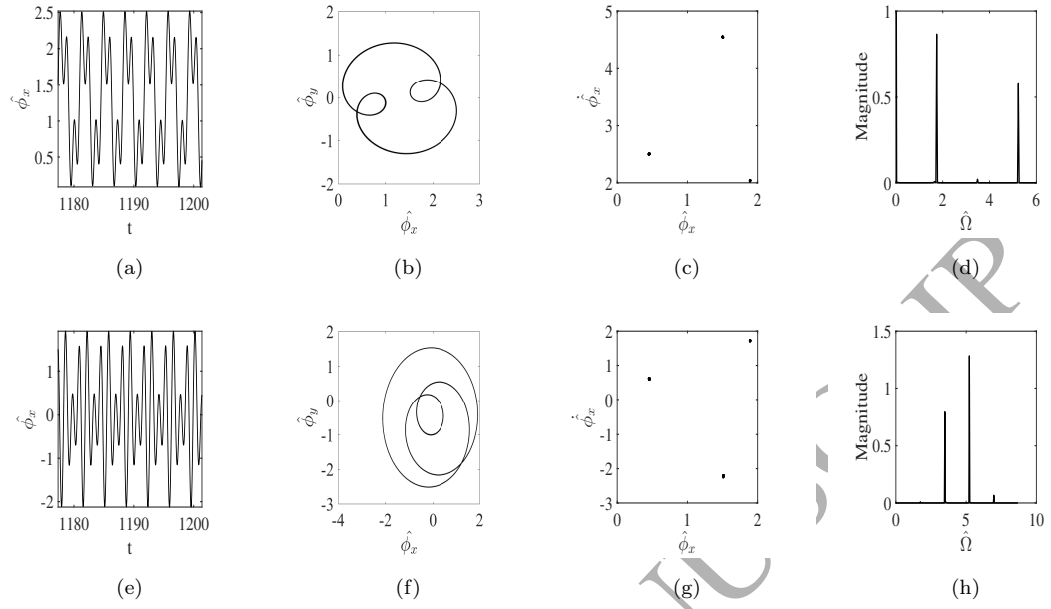

Figure 12: **Vibration responses (12a and 12e), phase trajectories (12b and 12f), Poincaré maps (12c and 12g) and amplitude spectra (12d and 12h) for $\hat{\Omega} = 5.23$ for $\hat{g} = 2.14$. Figures (12a - 12d) are for stationary frame and figures (12e - 12h) are for the rotating frame of reference.**

A closer look at the frequency components in Figure 13d shows three major peaks at 2.55, 1.18 and 1.559. To understand where these originate we examine the linear natural frequencies of the system from the Campbell diagram shown in Figure 6 at 2.55 and they were found to be 0.8342 and 1.1988. These are the BW and FW natural frequencies and these two frequencies are significantly different from those in the FFT because at $\hat{g} = 3.44$ the static deflection due to gravity dominates the response and thus there is a lot of stiffening due to the contact with the stator. Hence the natural frequencies of the linear stiffened system with complete contact are more representative of the motion; these natural frequencies are obtained using $(1+\beta)$ as the nondimensionalised stiffness in the linear and unforced versions of the equations of motion given by Equation (4). The values of BW and FW obtained for the stiffened system are 1.3517 and 1.7164 which are 10% and 14% higher than the corresponding FFT values. The FFT frequencies are slightly lower because the rotor is not always in contact whereas the natural frequencies of the stiffened system assume that contact is maintained.

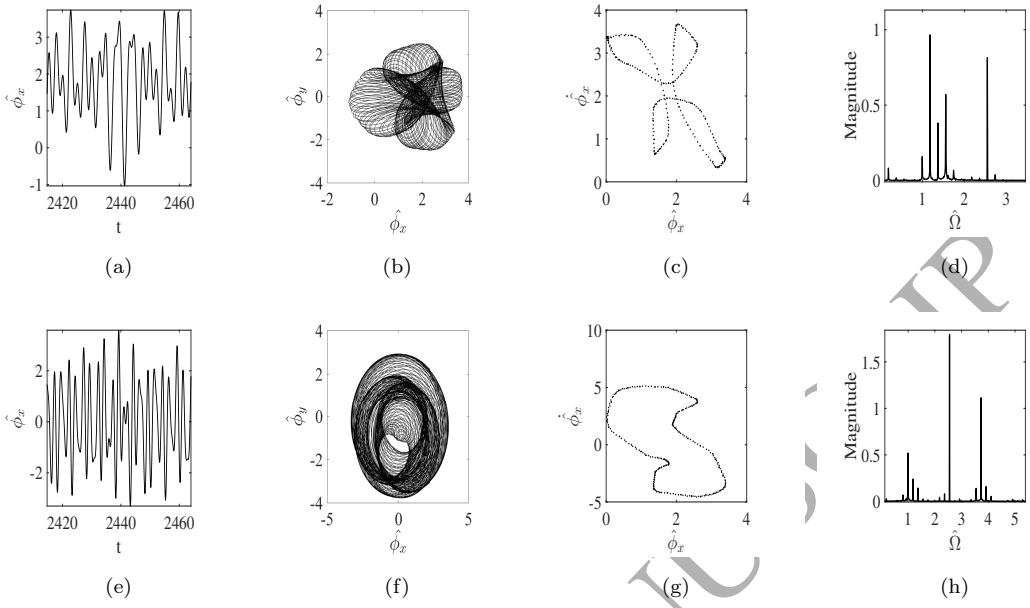

Figure 13: **Vibration responses (13a and 13e), phase trajectories (13b and 13f), Poincaré maps (13c and 13g) and amplitude spectra (13d and 13h) for $\hat{\Omega} = 2.55$ for $\hat{g} = 3.44$. Figures (13a - 13d) are for stationary frame and figures (13e - 13h) are for the rotating frame of reference.**

4. Conclusions

In this paper the effect of gravity on the nonlinear vibration phenomenon of an overhung rotor was investigated. The 4th order Runge Kutta method was used to obtain bifurcation diagrams, Lyapunov exponent spectra, amplitude spectra, orbit diagrams, phase trajectories and Poincaré maps that show the nonlinear behaviour of the rotor system. After nondimensionalising the equations of motion it was noted that the gravity parameter is a function of shaft stiffness. It was noted that when the shaft stiffness of the rotor is high, the gravity parameter is very small. This is the case explored in earlier studies and can be safely approximated to a zero gravity term. However, the opposite case of low shaft stiffness was explored in this study. The results presented here show that gravity introduces rich dynamic phenomenon into the rotor. For the zero gravity case the system only had periodic and quasi periodic solutions. Upon increasing the gravity parameter the system now exhibited multi-periodic and chaotic solutions. It was also observed that visualising the dynamic motion of systems in the rotating frame can give more insight into the nature of the

solutions particularly for the zero gravity case. The frequency content for the motion visualised in the rotating frame for the gravity case showed an additional peak not available in the zero gravity case showing that, in the rotating frame gravity is harmonic. It was also noted that rotor stator contact increases the effective stiffness(stiffening effect) and hence the shift in BW and FW natural frequencies. Lastly, the isotropic assumption for stiff rotors was found to be reasonably robust in the presence of imperfections since the orbits for the zero gravity case looked quite similar to that of $\hat{g}$=0.05 and 0.22.

Acknowledgements

The research leading to these results has received funding from Swansea University via the ZCCE PhD scholarship and the ENL EPSRC grant EP/K003836.

References

References

[1] F. F. Ehrich, Observations of nonlinear phenomena in rotordynamics, Journal of System Design and Dynamics 2 (2008) 641–651.

[2] K. Vijayan, N. Vlajic, M. I. Friswell, The influence of drillstring-borehole interaction on backward whirl, International Conference on Noise and Vibration Engineering, ISMA (2014).

[3] A. Zilli, R. J. Williams, D. J. Ewins, Nonlinear dynamics of a simplified model of an overhung rotor subjected to intermittent annular rubs, Journal of Engineering for Gas Turbines and Power 137 (2015) 065001.

[4] A. Shaw, A. Champneys, M. Friswell, Asynchronous partial contact motion due to internal resonance in multiple degree-of-freedom rotordynamics, in: Proc. R. Soc. A, volume 472, The Royal Society, 2016.

[5] W. Zhou, X. Wei, X. Wei, L. Wang, Numerical analysis of a nonlinear double disc rotor-seal system, Journal of Zhejiang University SCIENCE A 15 (2014) 39–52.

[6] H. Ma, X. Wang, H. Niu, B. Wen, Oil-film instability simulation in an overhung rotor system with flexible coupling misalignment, Archive of Applied Mechanics 85 (2015) 893–907.

[7] L. Yang, X. Chen, S. Wang, H. Zuo, Rub-impact detection of rotor systems using time-frequency techniques, in: ASME 2016 International Mechanical Engineering Congress and Exposition, American Society of Mechanical Engineers, 2016.

[8] C. Wang, D. Zhang, Y. Ma, Z. Liang, J. Hong, Theoretical and experimental investigation on the sudden unbalance and rub-impact in rotor system caused by blade off, Mechanical Systems and Signal Processing 76 (2016) 111–135.

[9] A. Muszynska, Rotor-to-stationary element rub-related vibration phenomena in rotating machinery: literature survey, The Shock and Vibration Digest 21 (1989) 3–11.

[10] A. Muszynska, D. Bently, W. Franklin, R. Hayahida, L. Kingsley, A. Curry, Influence of rubbing on rotor dynamics, Final Report NASA Contract No. NAS8 36719 (1989).

[11] A. Muszynska, W. D. Franklin, R. D. Hayashida, Rotor-to-stator partial rubbing and its effects on rotor dynamic response, NASA Report (1991).

[12] F. Chu, W. Lu, Experimental observation of nonlinear vibrations in a rub-impact rotor system, Journal of Sound and Vibration 283 (2005) 621–643.

[13] S. Lahriri, H. I. Weber, I. F. Santos, H. Hartmann, Rotor–stator contact dynamics using a non-ideal drive- theoretical and experimental aspects, Journal of Sound and Vibration 331 (2012) 4518–4536.

[14] J. Jiang, Y. Chen, Advances in the research on nonlinear phenomena in rotor/stator rubbing systems, Advances in Mechanics 43 (2013) 132–148.

[15] F. F. Ehrich, High order subharmonic response of high speed rotors in bearing clearance, ASME J. Vib., Acoust., Stress, Reliab. Des 110 (1988) 9–16.

[16] L. Hou, Y. Chen, Q. Cao, Nonlinear vibration phenomenon of an aircraft rub-impact rotor system due to hovering flight, Communications in Nonlinear Science and Numerical Simulation 19 (2014) 286–297.

[17] P. Varney, I. Green, Nonlinear phenomena, bifurcations, and routes to chaos in an asymmetrically supported rotor–stator contact system, Journal of Sound and Vibration 336 (2015) 207–226.

[18] J. Cao, C. Ma, Z. Jiang, S. Liu, Nonlinear dynamic analysis of fractional order rub-impact rotor system, Communications in Nonlinear Science and Numerical Simulation 16 (2011) 1443–1463.

[19] H. Khanlo, M. Ghayour, S. Ziaei-Rad, Chaotic vibration analysis of rotating, flexible, continuous shaft-disk system with a rub-impact between the disk and the stator, Communications in Nonlinear Science and Numerical Simulation 16 (2011) 566–582.

[20] J.-D. Jeng, L. Hsu, C.-W. Hun, C.-Y. Chou, Identification for bifurcation and responses of rub-impacting rotor system, Procedia Engineering 79 (2014) 369–377.

[21] G. Li, M. Paidoussis, Impact phenomena of rotor-casing dynamical systems, Nonlinear Dynamics 5 (1994) 53–70.

[22] Z. Feng, X.-Z. Zhang, Rubbing phenomena in rotor–stator contact, Chaos, Solitons & Fractals 14 (2002) 257–267.

[23] S. Strogatz, Nonlinear dynamics and chaos: with applications to physics, biology, chemistry, and engineering Cambridge, MA, Westview Press, 1994.

[24] A. Wolf, J. B. Swift, H. L. Swinney, J. A. Vastano, Determining lyapunov exponents from a time series, Physica D: Nonlinear Phenomena 16 (1985) 285–317.

[25] J. J. Thomsen, Vibrations and stability, order and chaos, McGraw-Hill Companies, 1997.

[26] A. H. Nayfeh, B. Balachandran, Applied nonlinear dynamics: analytical, computational, and experimental methods, in: Wiley Series in Nonlinear Sciences, John Wiley & Sons, Inc New York, 1995.

[27] F. C. Moon, Chaotic vibration: an introduction for applied scientists and engineers, New York.Chichester :Wiley, 2004.